Control strategies of human interactive robot under uncertain environments

Haiwei, Dong

Zhiwei, Luo

Control Strategies of Human Interactive Robot under Uncertain Environments

Haiwei Dong and Zhiwei Luo
Japan Society of the Promotion of Science and Kobe University
Japan

1. Introduction

Actually, the research on human interactive robot (HIR) has been a topic of both science fiction and academic speculation for a long time. The origin of HIR as a discrete issue was stated by 20th century author Isaac Asimov in 1941, in his novel "I, Robot". He stated the Three Laws of Robotics[1] as, "

a. A robot may not injure a human being or, through inaction, allow a human being to come to harm.
b. A robot must obey any orders given to it by human beings, except where such orders would conflict with the First Law.
c. A robot must protect its own existence as long as such protection does not conflict with the First or Second Law. "

The three laws of robotics determine the idea of safe interaction which constitutes the basic rules of HIR. With the advances of artificial intelligence (AI), the HIR could eventually have more proactive behaviours, planning their motion in complex unknown environments. Nowadays, HIR are artificial agents with capacities of perception and action in the human's environment. Their use has been tended to be found in the most technologically advanced societies in critical domains as search and rescue, military battle, law enforcement, entertainment, hospital care, etc. These domains of applications imply a closer interaction with human. The concept of closeness is to be taken in its full meaning, HIR and humans not only share the workspace but also share goals in terms of task achievement. The HIR has to adapt itself to human's way of expressing desires and fulfill its task. Taking lifting up human in elder care for example, the human interactive robot RI-MAN, designed by the RIKEN Bio-Mimetic Control Research Center, communicates with human by listening and speaking, which makes it understand the human will (Onish, Luo et al. 2007). To fulfil the task, it also estimates the attitude of human body in real-time by tactile sense (Mukai, Onishi et al. 2008). This example contains two aspects of HIR, one is to understand the human mind and the other is to accomplish the manipulation. The former is based on AI techniques, like language comprehension, and the latter is relied on force control.

On the other hand, human's environments are much more complex. Thus, the HIR needs perceiving and understanding capacities to build dynamic models of its surroundings. It

[1] In science friction, the Three Laws of Robotics are a set of three rules written by Isaac Asimov, which almost all positronic robots appearing in his friction must obey.

needs to categorize objects, recognize and locate humans and further their emotions. Also in the case of human interactive robot RI-MAN (Mukai, Onishi et al. 2008), if he cannot navigate in the hospital and further more cannot locate the human, the understanding and good manipulation mentioned above make no sense. In our opinion, with the development of human society and robotics technology, HIR research becomes much important (Fig. 1).

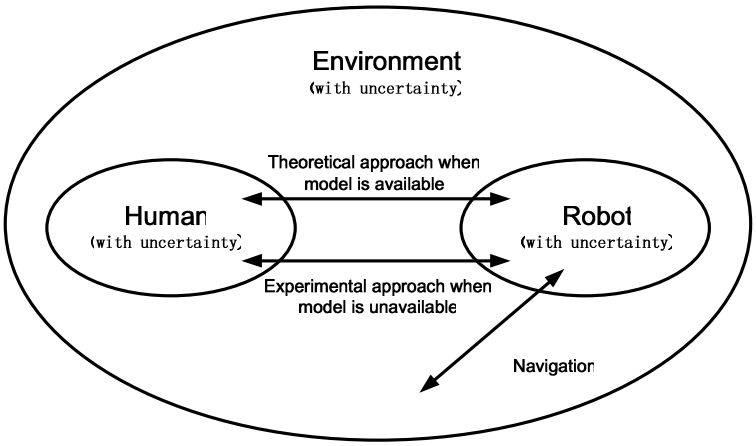

Fig. 1. Interaction relation between human, robot and environment.

As HIR interacts with human, sometimes we can model the process of human activity accurately and the robot-human interaction process can be simulated and further done by theoretical approach; sometimes human movement is too complex to model and in that case, the experimental approach is a good way. However, the above thing is to make the HIR capable to navigate in the human environment.

The chapter focuses on the issue of designing control strategies of human interactive robot where dealing with uncertainties is a critical issue. Actually, although there are many researches on HIR, these works do not concern too much on the uncertainty. The fact is that there are various uncertainties in the world which comes from robot, human, environment, etc. Developing human interactive robot, in some concept, is dealing with uncertainties. Actually, there are kinds of solving approaches for uncertainties according to circumstances: some uncertain can be assumed as Gaussian noise and based on the property of Gaussian noise, we can do estimation more accurately; some uncertainty coming from model reduction and this kind of uncertainty can be solved by control theory; some uncertainty is neither hard to model, nor difficult to determine the source. In that case, it is a better way to consider it as a black box and recognize it by system identification.

In our opinion, the issue of uncertainty has become a major stumbling block for the design of capable human interactive robot. To develop a human interactive robot, it is evitable to deal with uncertainties. Furthermore, managing uncertainty is possibly the most important step towards robust real-world HIR systems (Thrun, Burgard et al. 2005). The basic principle of this chapter is to design control for HIR by dealing with uncertainties. Specifically, there are a number of factors that contribute to the uncertainty of robot, human and environment:

Firstly, robot environment is inherently unpredictable. While the degree of uncertainty in well-structured environment such as assembly lines is small, environments such as

highways and private homes are highly dynamic and in many ways highly unpredictable. The uncertainty is particularly high for robots to operating in the proximity of people.

Secondly, sensors are limited in what they can perceive. Limitations arise from several factors. The range and resolution of a sensor is subject to physical limitations. For example, cameras cannot see through walls, and the spatial resolution of a camera image is limited. Sensors are also subject to noise, which perturbs sensor measurements in unpredictable ways and hence limits the information that can be extracted. And finally, sensors can break. Detecting a faulty sensor can be extremely difficult.

Thirdly, robot actuation involves motors that are, at least to some extent, unpredictable. Uncertainty arises from the physical structure of actuator, i.e. actuator is impossible to achieve absolute precision. In addition, uncertainty also comes from control noise, wear-and-tear, mechanical failure, etc.

Fourthly, some uncertainty is caused by model approximation. Models are abstractions of the real world. As such, they only partially model the underlying physical process of the subject. Model errors are a source of uncertainty that has a great impact on the fulfillment of the robot task.

Fifthly, there are some uncertainties that are extremely difficult to model or are impossible to obtain. In that case, the uncertainty is very hard to deal with by analytic methods, like mathematical approaches. Also the evaluation of the uncertainty, both sources and magnitude are hard to be obtained.

In summary, the uncertainties caused by the five factors can be noted as environment uncertainty, sensor uncertainty, actuator uncertainty, model uncertainty, unmodeled uncertainty, respectively. The above five kinds of uncertainties involve nearly all the uncertainties human interactive robot may encounter. The control design of HIR in this chapter takes it a clue to deal with the uncertainties mentioned above. In other words, we correlate the basic HIR's technical problems with the five uncertainties. By dealing with the uncertainties, we design control for HIR and finally solve the basic technical problems of HIR. Specifically, the first basic problem is to make HIR capable to navigate in a large unknown environment which corresponds to dealing with environment uncertainty, sensor uncertainty and actuator uncertainty; the second basic problem is to propose approach for HIR to physically interact with human which has large degrees of freedom (DOF). This basic problem corresponds to dealing with the model uncertainty. The third basic problem is to design approach for HIR to mentally interact with human, i.e. extract the human's intention, which corresponds to dealing with unmodeled uncertainty. The detailed explanation on correlation between the basic problems and corresponding uncertainties is as follows:

The first basic problem concerns two issues as robot localization and environment cognition, i.e. to estimate the robot's position and the feature's position. Considering that robot's motion and observation are affected by Gaussian noise, its kinematics model and sensor model are added by uncertainty. Similarly, the position of feature (or landmark from the viewpoint of mapping) is also affected by Gaussian noise; herein we add Gaussian uncertainty in the model. With regards to these models with uncertainty, it is better to use a probabilistic approach to estimate robot's and landmark's positions, i.e. simultaneous localization and mapping (SLAM). By definition, SLAM is the process by which a mobile robot builds a map of an environment and at the same time uses this map to compute its own location. By SLAM, robot is able to navigate in an unknown environment freely. However, the problem is that the current SLAM approaches only fit the relative small

environment because of the time-consuming computation. When solving the first basic problem, the main topic is to propose an efficient SLAM approach for large scale unknown environment.

The second basic problem contains two issues potentially: the interactive object is human dynamics with large degree of freedom; the interactive manipulation is physically done by force. As the first issue, human body has numerous bones and joints and the human model is a very complex one with large degrees of freedom. Exerting force on such a big model is very complex and such dynamic process is impossible to be calculated in real time. Here we use model reduction to decrease the DOF of human model whereas the reduction error (i.e. model uncertainty) comes out. For the second issue, external force is exerted on human. Unlike common object, human has passive moment in human joint and more complicated, sometimes moves at his or her will. Such force character provides a big challenge to control. To solve the basic problem two, the main topic is to propose an adaptive force control approach for HIR when physically contacting with human. More specifically, we take a typical case to research, i.e. how to lift human by HIR in nursing care.

The third basic problem focuses on obtaining the human's intention. Actually, the human's intention is very difficult to measure. The model for human mind is also extremely hard to build right now. For us, the human's intention is almost full of unmodeled uncertainty, i.e., we have little knowledge about it. In this case, treating it as a black box is a good way. We stimulate the black box (i.e. human dynamics system) and measure output. By choosing a suitable function to link the stimulus signal and output, we can obtain the intention model experimentally. The main topic here is to design an approach for extracting human's intention. Without loss of generality, in this chapter we consider the problem of estimating the human's intended walking speed.

To conclude, in this chapter, we design controls for human interactive robot by dealing with the environment uncertainty, sensor uncertainty, actuator uncertainty, model uncertainty and unmodeled uncertainty. Specifically, the typical problems of HIR we focus on are designing an efficient SLAM approach for large unknown environment; proposing an adaptive force control for lifting human up; estimating human's intended walking speed. The above three typical problems involve the basic problems when designing controls for HIR. The solution of them also provides a general solving framework for HIR, which is of great importance both in research and in application. The preceding researches relating with the above three typical problems are shown as follows.

2. Motion control for large environment navigation

2.1 Background

Extended Information Filter SLAM (EIF-SLAM) estimates the positions of robot and landmarks by updating information matrix and information vector. The total element numbers of information matrix and information vector are

$$\left(dof\left(landmark\right)\times n_{lm}+dof\left(robot\right)\right)^2$$

and

$$dof\left(landmark\right)\times n_{lm}+dof\left(robot\right)$$

where n_{lm} denotes the mapped landmarks. $dof(landmark)$ and $dof(robot)$ denote landmarks' degree of freedom (DOF) and robot's DOF, respectively. Actually, the dimension of the information matrix increases rapidly with the increase of the landmark number in the environment. For example, if a three-dimensional environment has 100 landmarks, the information matrix is a huge matrix with dimension of 303 by 303. Actually, the computational burden in EIF-SLAM is mainly due to the calculation of the information matrix.

Previous research has proven that information matrix is a naturally sparse matrix (Eustice, Singh et al. 2005). Hence, it is a good way to make use of this feature and change information matrix into a real sparse matrix for computation reduction. Until now, the successful research includes Thrun et al.'s work which solved a relatively large environment (i.e. Victoria Park) for the first time (Thrun, Koller et al. 2002); Eustice et al.'s work which constructed the map of Titanic ship in the dark ocean (Eustice, Singh et al. 2005). Among this work, the sparsification of information matrix was obtained by constructing a proper topological structure of Bayes network, which needs to classify the landmarks in advance. This is a time-consuming work and against the enhancement of efficiency. Actually, the intuitive idea is to set the near-zero elements to zero directly. Thrun tried this way (Thrun, Liu et al. 2004), however, Eustice proved that direct sparsification leads the algorithm diverge (Eustice, Walter et al. 2005), which indicates the improper sparsification process mentioned may cause the algorithm corrupt. If we want to pursue this kind of idea, we have to clarify the condition under which the algorithm maintains stable which constitutes the basis of this section. This section focuses on proposing an efficient stable sparsification SLAM approach for large scale environment.

2.2 Sparsing information matrix

2.2.1 Characters of information matrix

In fact, information matrix in EIF-SLAM has special structural characters (Dong, Luo et al. 2009) where the value denotes the numerical value of the element in information matrix located at $(row\ index,\ column\ index)$. It is convenient to divide the elements of information matrix into two parts: Part I denotes larger part where the elements have larger values. The elements along the main-diagonal and near the endpoints of sub diagonal line belong to this part. Part II is composed of other elements in the information matrix. Three main characters of information matrix can be stated as

a. Information matrix is symmetric along the main diagonal line;
b. Elements with huge values distribute in the neighborhood of the main diagonal line and the end points of the sub diagonal line (Part I);
c. For the elements of Part II, the value of the element decreases with the distance from the main diagonal line.

The reasons for character 1) to 3) can be explained as follows, respectively (Smith, Self et al. 1990; Liu and Thrun 2003; Eustice, Singh et al. 2005; Eustice, Singh et al. 2006).

a. Each element in the information matrix denotes the link strength between the corresponding landmark and robot. As we all know that the link strength has symmetry, i.e. if the link strength between A and B is π, then the link strength both from A to B and from B to A are π. Therefore, information matrix is a symmetric matrix;

b. From the viewpoint of Bayes network, the link strength shows the correlation. In SLAM problem, the largest correlation is the relation of robot itself and landmark itself. The correlation between the robot and landmark becomes weak with time. If the robot is currently observing a landmark, the correlation between the robot and the landmark is strong. The elements in diagonal line denote the link strength of robot versus itself, or landmark versus itself while the elements near the endpoint of information matrix show the link strength of robot versus current observing landmark. Hence, the elements with large value centralize in Part II;

c. The correlation becomes weak when time passes after observing it. When the robot observes the landmark again, the correlation increases again.

The most important characteristic of information matrix is that most elements of it are nearly zero. In other words, an information matrix is a nearly sparse matrix. The information matrix sparsification by different threshold χ_i $(1 \le i \le 6)$ is shown in Fig. 2 where χ_i is

$$\begin{cases} \chi_{i+1} = 10^2 \times \chi_i \\ \chi_1 = 10^{-13} \end{cases} \quad (1 \le i \le 5) \tag{1}$$

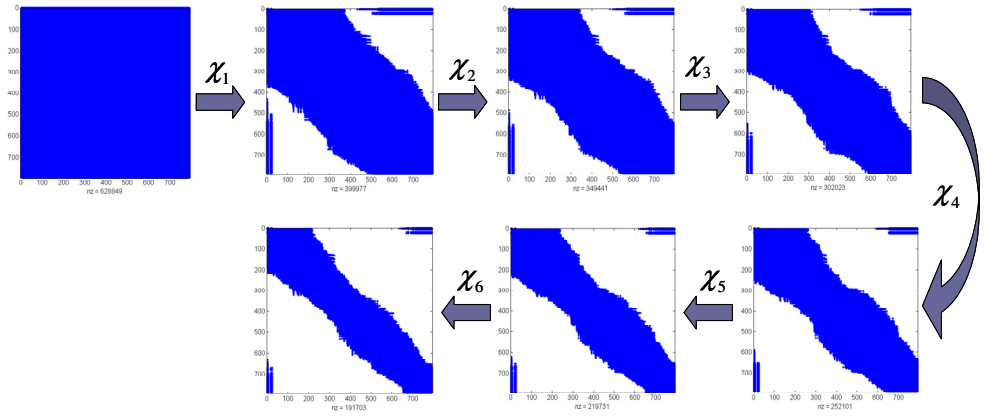

Fig. 2. Information matrix sparsification.

After computing the sparse ratios of the information matrices in Fig. 2, we can get the graph that illustrates how the sparse ratio changes with the threshold (Fig. 3) where the x-axis denotes the threshold and the y-axis denotes the sparse ratio. By using a curve fitting method, it shows that the distribution of elements in the information matrix satisfies a linear distribution in logarithmic coordinates. The sparse ratio increases with the threshold. However, sparsification error arises from the sparsification process. Furthermore, inappropriate sparsification may lead EIF-SLAM to diverge. Therefore, the key issue here is to find a condition under which the estimation results converge all the time.

From the illustrations above, the information matrix in EIF-SLAM algorithm is naturally sparse. Hence, the sparsification structure of the information matrix is very suitable to be sparsed. Moreover, because the computations are mainly on the calculation relating with

information estimation variables, high efficiency is predicted by sparsing the information matrix. The following sparsification approach utilizes the characters of the information matrix to decrease the computational burden of EIF-SLAM.

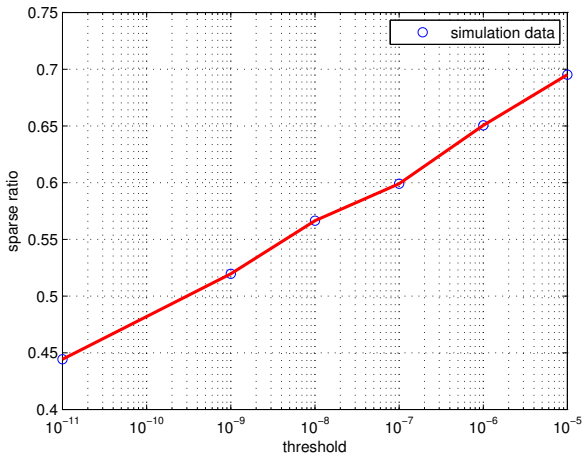

Fig. 3. Linear relation between sparse ratio and threshold.

From the illustrations above, we obtain that the information matrix in EIF-SLAM algorithm is naturally sparse. Hence, the sparsification structure of the information matrix is very suitable to be sparsed. Moreover, because the computations are mainly on the calculation relating with information estimation variables, high efficiency is predicted by sparsing the information matrix. The following sparsification approach utilizes the characters of the information matrix to decrease the computational burden of EIF-SLAM.

2.2.2 Sparsification approach

The mean vector μ and the covariance matrix Σ of the environment state vector ε are written in the form

$$\varepsilon = \begin{bmatrix} \varepsilon_1 \\ \varepsilon_2 \\ \vdots \\ \varepsilon_n \end{bmatrix}, \mu = \begin{bmatrix} \mu_1 \\ \mu_2 \\ \vdots \\ \mu_n \end{bmatrix}, \qquad \Sigma = \begin{bmatrix} \sigma_{11} & \sigma_{12} & \cdots & \sigma_{1n} \\ \sigma_{21} & \sigma_{22} & \cdots & \sigma_{2n} \\ \vdots & \vdots & \ddots & \vdots \\ \sigma_{n1} & \sigma_{n2} & \cdots & \sigma_{nn} \end{bmatrix} \tag{2}$$

Assume estimation error is a Gaussian noise, we have

$$\begin{aligned} &\mathrm{Prob}\left(\max_{1\le i\le n}\{|\mu_i-\varepsilon_i|-\sigma_{ii}\}\le 0\right)\approx 0.68 \\ &\mathrm{Prob}\left(\max_{1\le i\le n}\{|\mu_i-\varepsilon_i|-2\sigma_{ii}\}\le 0\right)\approx 0.95 \\ &\mathrm{Prob}\left(\max_{1\le i\le n}\{|\mu_i-\varepsilon_i|-3\sigma_{ii}\}\le 0\right)\approx 0.997 \end{aligned} \tag{3}$$

By taking the relation between time estimation variables and information estimation variables

$$\begin{cases} \Lambda^{-1}\eta = \mu \\ \Lambda^{-1} = \Sigma \end{cases} \tag{4}$$

into Equation (3), we obtain

$$\begin{aligned} &\mathrm{Prob}\left(\max\left\{\left|\Lambda^{-1}\eta - \varepsilon\right| - \mathrm{Sqrt}\left(D(\Lambda^{-1})\right)\right\} \le 0\right) \approx 0.68 \\ &\mathrm{Prob}\left(\max\left\{\left|\Lambda^{-1}\eta - \varepsilon\right| - 2\times\mathrm{Sqrt}\left(D(\Lambda^{-1})\right)\right\} \le 0\right) \approx 0.95 \\ &\mathrm{Prob}\left(\max\left\{\left|\Lambda^{-1}\eta - \varepsilon\right| - 3\times\mathrm{Sqrt}\left(D(\Lambda^{-1})\right)\right\} \le 0\right) \approx 0.997 \end{aligned} \tag{5}$$

Here we propose Theorem 1 to clarify the conditions for sparsification for guaranteeing the convergence. In other words, from the viewpoint of mathematics, Theorem 1 gives the consistency condition; from the viewpoint of geometric, the mean remains in the range of the corresponding covariance under consistency condition.

Theorem 1

Assume the new information matrix after sparsification is written in the form of $\Lambda + E$, where E is the sparsification error matrix. If $\max\left\{\left(\Lambda^{-1}\eta - \varepsilon\right) \otimes H\eta\right\} \le 0$ is satisfied, we obtain

$$\max\left\{\left|(\Lambda + E)^{-1}\eta - \varepsilon\right| - \mathrm{Sqrt}\left(D(\Lambda^{-1})\right)\right\} \le 0 \tag{6}$$

where

$$\begin{aligned} H &= -\bar{\Sigma}\left(I + \underline{\bar{E}}\bar{\Sigma}\right)^{-1}\underline{\bar{E}}\underline{\Sigma} \\ &= -\bar{\Sigma}\bar{\underline{E}}\left(I + \bar{\Sigma}\bar{\underline{E}}\right)^{-1}\underline{\Sigma} \end{aligned} \tag{7}$$

$\bar{\underline{\Sigma}}$, $\bar{\Sigma}$, $\underline{\Sigma}$ and $\bar{\underline{E}}$ are defined as

$$\Sigma = \begin{bmatrix} \bar{\underline{\Sigma}} & \Sigma_2 \\ \Sigma_1 & \Sigma_3 \end{bmatrix}, \quad E = \begin{bmatrix} \underline{\bar{E}} & 0 \\ 0 & 0 \end{bmatrix}, \quad \bar{\Sigma} = \begin{bmatrix} \bar{\underline{\Sigma}} \\ \Sigma_1 \end{bmatrix}, \quad \underline{\Sigma} = \begin{bmatrix} \bar{\underline{\Sigma}} & \Sigma_2 \end{bmatrix} \tag{8}$$

where the element positions of $\bar{\underline{\Sigma}}$ are the transport element position of $\underline{\bar{E}}$. That is, the portioned matrices $\underline{\bar{E}}$, $\bar{\underline{\Sigma}}$, $\bar{\Sigma}$ and $\underline{\Sigma}$ are of order of $m_1 \times m_2$, $m_2 \times m_1$, $n \times m_2$ and $m_1 \times n$, respectively.

The proof of Theorem 1 is shown in (Dong, Tang et al. 2010). Consider Equation (6) with respect to Equation (5), it is shown that after sparsification, each estimated mean still inside the scope of corresponding covariance. That is to say, the estimated position of the robot or landmark is inside the estimation range, which indicates the estimation is reliable. In addition, the proof of Theorem 1 also gives a quite efficient way to get covariance matrix

from information matrix without directly computing the inversion. According to Theorem 1, we can eliminate the information matrix under the condition of stabilization. In practice, loop-closure is used to compensate the estimation error which comes from sparsification. After sparsification, another theorem was proposed to evaluate sparsification error by deriving the upper bound of relative error ratios, including mean vector error ratio and covariance matrix error ratio (Dong, Tang et al. 2010).

2.3 Large complex environment simulation

The proposed sparsification SLAM approach was simulated in a large scale environment (about 400 landmarks). As the landmarks are very dense, the environment is a complicated one. Such environment can further verify the effectiveness of the proposed approach. In the simulation, the robot applied is a two-wheel robot with three degrees of freedom and the sensor arranged on the robot is range-bearing type sensor (such as laser, camera, etc.). The robot moves counterclockwise for two laps while utilizing sparsification approach to process SLAM.

2.3.1 Efficiency analysis

The main computational burden of EIF-SLAM is primarily from the three steps: motion update, features addition and observation update. The comparison of computational time between EIF-SLAM (denoted as stars) and sparsification method (denoted as crosses) is shown in Fig. 4. It shows that the sparsification approach is able to solve SLAM in the environment with 400 landmarks. Furthermore, according to the curve trend of computational time, we can predict that our sparsification method has an efficiency advantage for large environment.

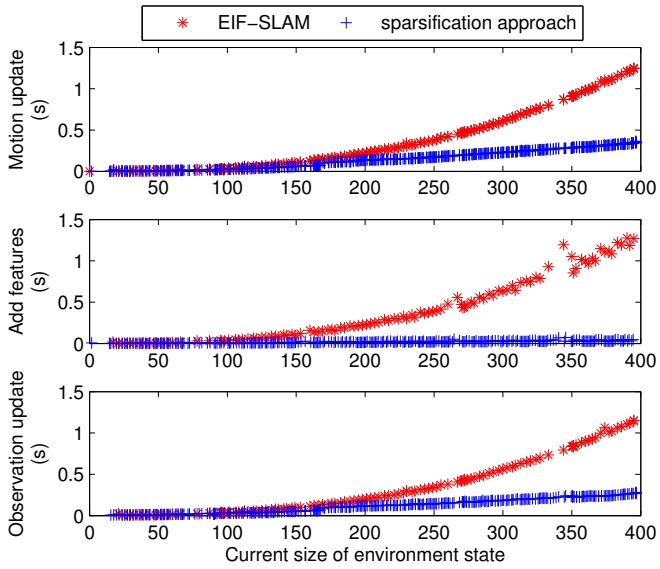

Fig. 4. Efficiency comparison between EIF-SLAM and sparsification SLAM.

2.3.1 Accuracy analysis

The comparison of error and covariance is shown in Fig. 5 where dash line and solid line denote estimation error and self-covariance of robot's position, respectively. Horizontal axis shows the time. Vertical axis denotes the estimation error and covariance where x and y denote the moving directions, respectively. It shows that estimation error and covariance decrease sharply at time 250, which indicates that there is a loop-closure at this moment.

In fact, during the first lap, the error and covariance by the sparsification method nearly have the same magnitude, (in Fig.5 (b), the solid line nearly coincides with the dash line), which indicates that the sparsification method eliminates considerable number of elements under the condition of consistency. In the second lap, the estimation error by EIF-SLAM (Fig. 5 (a)) and the sparsification approach (Fig. 5 (b)) seems the same. Thus, it can be concluded that by using loop-closure properly, the sparsification approach can obtain satisfying accuracy with high efficiency.

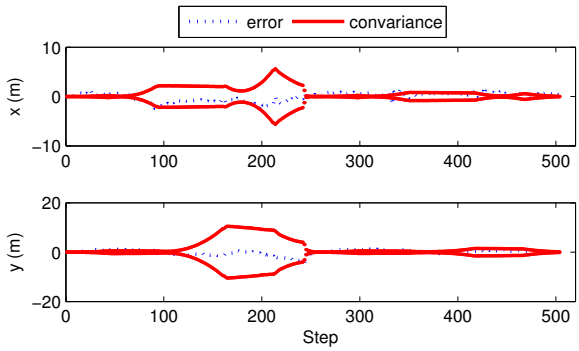

a)

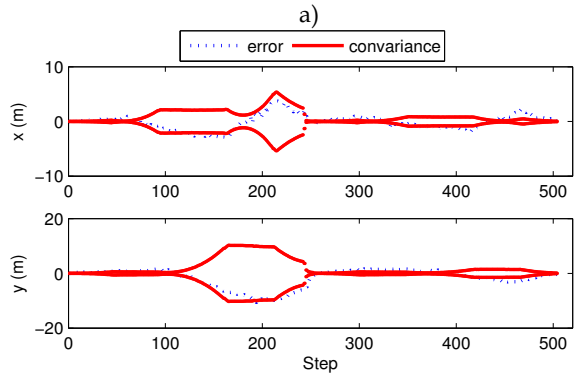

b)

Fig. 5. Comparison of estimation error and covariance.

2.4 Summary

In this section, a sparsification EIF-SLAM approach was proposed to enable human interactive robot to navigate in the large unknown environment. According to the normal structural features of information matrix, we eliminate many of the near-zero elements in the information matrix. Such sparsification process is under the condition of consistency.

Hence the sparsification approach stays stable. In addition, the upper bound of estimation error is also given for evaluation. The large complex environment simulation indicates that the sparsification approach has the advantage of high efficiency and accuracy. The outdoor car-park experiment shows the ability to realize consistent estimation by the sparsification approach (Dong, Luo et al. 2009).

Compared to the previous researches on efficient navigation of human interactive robot, the sparsification approach proposed in this section gives a direct but effective way to obtain efficiency. Concerning parameters, we can compromise the efficiency and accuracy under the condition of stabilization. It is also noted that the consistency condition derived in this section also has great meaning for the future research on sparsification.

This section dealt with the environment uncertainty, sensor uncertainty, actuator uncertainty, and assumed them as Gaussian noises. The proposed sparsification SLAM approach eliminated these uncertainties and realized high efficiency of SLAM estimation.

3. Adaptive force control for lifting human

3.1 Background

It has been thought that the human body is composed of 206 bones and numerous human joints connecting adjacent bones. Based on the physiological structure of human joints, the human joints can be mainly divided into three types as the hinge (1 DOF), the pivot (1 DOF) and the ball socket (3 DOF). In dynamic equations, each DOF is expressed as one differential equation, which indicates that the overall set of equations of human body dynamics is a very huge one. The force interaction with such a big model needs considerable computation for human interactive robot.

As illustrated in Section 1, in the process of lifting human, the human body has to be considered as a free-floating multi-link rigid object with passive moments. Compared with one-end-fixed object, like manipulator, free-floating object is much more complex. The force acting on any part of the object would affect the attitude of the entire object. Moreover, although the multi-link object has been researched a lot, the one with large DOF and large redundancy has not fully been considered yet. Another problem is calculation; any computation on such a huge model needs much computational time whereas the safe lifting requires real-time computation.

In consideration of the difficulties mentioned above, our basic idea for lifting human comes from the daily experience. When we human lift a person, we do not care too much about the detailed dynamics, like the change of ankle angle, hand position and so on. What we do care about are the head position, the vertical deflection of upper limb and the hip angle. Here we call them “states of interest”. From the viewpoint of system theorem, we treat the human body as a large redundant system whose dimensions are reduced by diverting the effects of other “joints of noninterest” to the “interested ones”. The resulting body model is a reduced one with less DOF but unfortunately, has huge uncertainties (i.e. model uncertainty). Here we focus on proper model reduction and methods for dealing with the generating model uncertainty, which leads to a force control for lifting human.

3.2 Force interaction modeling

If we consider human body as a rigid multi-link object, each bone corresponds to a link and each human joint corresponds to a joint connecting adjacent links. Moreover, human joints

have passive torques corresponding to the constriction forces and moments developed by ligaments, joint capsules and other soft tissues. Hence, we write the dynamics of human in the from

$$H(q)\ddot{q} + C(q,\dot{q})\dot{q} + G(q) = \tau_{pass}, \tag{9}$$

where

$q_{n\times 1}$ Generalized body states, including the position of head and the angles of all the joints.

$H(q)_{n\times n}$ Inertia matrix, defined as a positive semi-definite symmetric matrix, containing information on the body's instantaneous mass distribution.

$C(q,\dot{q})_{n\times n}$ Centripetal and coriolis torques. $C(q,\dot{q})$ term contains products of angular speeds. When the degree of freedom is rotational, the terms of $C(q,\dot{q})$ represent the moments of centrifugal forces.

$G(q)_{n\times 1}$ Gravitational torques. Because $G(q)$ changes as the posture configuration of the human body model, its terms are functions of the generalized states.

$\tau_{pass\ n\times 1}$ Passive joint torque, including torques and moments arising from muscular activations and passive elastic structures surrounding the human joints.

Here the HIR's task is to lift human, i.e. to control the position and posture of the body to the desired states by external forces. Adding the force exertion in Equation (9), leads to:

$$H(q)\ddot{q} + C(q,\dot{q})\dot{q} + G(q) = \tau_{pass} + \tau_{rob}, \tag{10}$$

where $\tau_{rob\ n\times 1}$ The torques acted by the robot arms which is controllable.

Actually, the human interactive robot considered in this section has two manipulation arms, like RI-MAN (Mukai, Onishi et al. 2008). Force is applied to the fixed point at back and knees, shown as F_1 and F_2. Forces F_1 and F_2 have relations with τ_{rob} as

$$\tau_{rob} = J_1{}^T F_1 + J_2{}^T F_2, \tag{11}$$

where J_1 and J_2 are the Jacobian matrices of the human body model.

3.3 Human dynamics reduction

The basic idea in this section is to reduce the human body model into a small one with less degree of freedom, which includes the following three steps:

a. Choose "states of interest". These states include the fundamental performance indexes of the task. In other words, based on these states, we can determine whether the task is complete or not and furthermore, evaluate the performance is good or not. Let us define

$$\bar{q}_1 = \left[q_1,\cdots,q_m\right]^T_{m\times 1} \tag{9}$$

as the "states of interest" and

$$\bar{q}_2 = \left[q_{m+1},\cdots,q_n\right]^T_{(n-m)\times 1} \tag{10}$$

as the "uninterested states" consisting of the other states. The overall state can be written as $q=[\bar{q}_1 \quad \bar{q}_2]^T$.

b. Arrange the dynamic equation set. Based on the division of generalized states in (a), we change the element position of H, C, G, τ_{pass}, τ_{rob}. The expanded form of new dynamics equation set is

$$\begin{bmatrix} \bar{H}_{11} & \bar{H}_{12} \\ \bar{H}_{21} & \bar{H}_{22} \end{bmatrix} \begin{bmatrix} \ddot{\bar{q}}_1 \\ \ddot{\bar{q}}_2 \end{bmatrix} + \begin{bmatrix} \bar{C}_{11} & \bar{C}_{12} \\ \bar{C}_{21} & \bar{C}_{22} \end{bmatrix} \begin{bmatrix} \dot{\bar{q}}_1 \\ \dot{\bar{q}}_2 \end{bmatrix} + \begin{bmatrix} \bar{G}_1 \\ \bar{G}_2 \end{bmatrix} = \begin{bmatrix} \bar{\tau}_{pass,1} \\ \bar{\tau}_{pass,2} \end{bmatrix} + \begin{bmatrix} \bar{\tau}_{rob,1} \\ \bar{\tau}_{rob,2} \end{bmatrix}, \tag{11}$$

where the dimensions of sub block matrices of $\bar{H}_{11}$, $\bar{H}_{12}$, $\bar{H}_{21}$, $\bar{H}_{22}$ are $m\times m$, $m\times(n-m)$, $(n-m)\times m$, $(n-m)\times(n-m)$, respectively. The dimensions of the sub block matrices $\bar{C}_{11}$, $\bar{C}_{12}$, $\bar{C}_{21}$, $\bar{C}_{22}$ are $m\times m$, $m\times(n-m)$, $(n-m)\times m$, $(n-m)\times(n-m)$, respectively. The dimensions of vectors $\bar{G}_1$, $\bar{\tau}_{pass,1}$, $\bar{\tau}_{rob,1}$ are $m\times 1$, and $\bar{G}_2$, $\bar{\tau}_{pass,2}$, $\bar{\tau}_{rob,2}$ are $(n-m)\times 1$.

c. Construct the small dynamics equation set. First of all, we define the generalized states of reduced model as

$$q_s=\bar{q}_1 \tag{12}$$

Then extracting the parts of the human dynamics relating with q_s, we get

$$\begin{bmatrix} \bar{H}_{11} & \bar{H}_{12} \end{bmatrix} \begin{bmatrix} \ddot{\bar{q}}_1 \\ \ddot{\bar{q}}_2 \end{bmatrix} + \begin{bmatrix} \bar{C}_{11} & \bar{C}_{12} \end{bmatrix} \begin{bmatrix} \dot{\bar{q}}_1 \\ \dot{\bar{q}}_2 \end{bmatrix} + \bar{G}_1 = \bar{\tau}_{pass,1} + \bar{\tau}_{rob,1} \tag{13}$$

Considering that the dynamic model is time-varying, after arranging Equation (13), we obtain

$$\bar{H}_{11}(t)\ddot{\bar{q}}_1 + \bar{C}_{11}(t)\dot{\bar{q}}_1 + \left(\bar{G}_1(t) + \bar{H}_{12}(t)\ddot{\bar{q}}_2 + \bar{C}_{12}(t)\dot{\bar{q}}_2 - \bar{\tau}_{pass,1}(t)\right) = \bar{\tau}_{rob,1}(t) \tag{14}$$

By defining the inertia matrix, centripetal matrix, gravitational matrix and torque vector of the reduced human dynamics as

$$\begin{aligned} H_s(t) &= \bar{H}_{11}(t) \\ C_s(t) &= \bar{C}_{11}(t) \\ G_s(t) &= \bar{G}_1(t) + \bar{H}_{12}(t)\ddot{\bar{q}}_2 + \bar{C}_{12}(t)\dot{\bar{q}}_2 - \bar{\tau}_{pass,1}(t) \\ \tau_s(t) &= \bar{\tau}_{rob,1}(t) \end{aligned} \tag{15}$$

we obtain the general mechanical form of the reduced human dynamics

$$H_s(t)\ddot{q}_s + C_s(t)\dot{q}_s + G_s(t) = \tau_s(t) \tag{16}$$

where the subscript s denotes the small system. We consider the influences from "uninterested human joints" (in this case from state $\bar{q}_2$) as perturbations.

We change the attitude of reduced human model adaptively by estimating the parameters of H_s, C_s and G_s in real time. The detailed estimation meanings are as follows.

- Estimating H_s and C_s --- make the system adaptively adjust itself to various people with different weights.

- Estimating G_s --- eliminate the perturbations from other "uninterested joints".

Considering the basic principle above, the approach to be proposed in this section is to identify and control the reduced human dynamics at the same time. Assuming that the human parameters are totally unknown in advance, for the safety in the nursing activity, the identification process needs to be performed in real time. On the other hand, the weights and heights etc. of the human bodies are different between individuals. Hence, the strategy also has to be able to tolerate these individual difference.

3.4 Attitude control and human parameter identification

First of all, we assume that we do not have any priori knowledge before lifting human, i.e. the initial value of H_s, C_s, G_s are set to be zero matrices and zero vectors. The benefit of such assumption is that the proposed trajectory is much more robust and can be adaptive to various people with different heights and weights. Whereas, such assumption also leads to a problem, i.e. it generates much model uncertainties in the dynamics. To solve the above problem, we use robust controller to change the human attitude to the desired states. Moreover, online human parameter identification is also done so as to estimate the human body in real time.

For the convenience of mathematical derivation, we define the actual human parameter vector

$$P = \begin{bmatrix} P_H^T & P_C^T & P_G^T \end{bmatrix}^T \tag{17}$$

where

$$P_H = \begin{bmatrix} H_{s,11} & H_{s,12} & \cdots & H_{s,1n} & \cdots & H_{s,n1} & H_{s,n2} & H_{s,nn} \end{bmatrix}^T \tag{18}$$

$$P_C = \begin{bmatrix} C_{s,11} & C_{s,12} & \cdots & C_{s,1n} & \cdots & C_{s,n1} & C_{s,n2} & C_{s,nn} \end{bmatrix}^T \tag{19}$$

$$P_G = \begin{bmatrix} G_{s,1} & G_{s,2} & \cdots & G_{s,n} \end{bmatrix}^T \tag{20}$$

and estimated human parameter vector as

$$\hat{P} = \begin{bmatrix} \hat{P}_H^T & \hat{P}_C^T & \hat{P}_G^T \end{bmatrix}^T \tag{21}$$

where

$$\hat{P}_H = \begin{bmatrix} \hat{H}_{s,11} & \hat{H}_{s,12} & \cdots & \hat{H}_{s,1n} & \cdots & \hat{H}_{s,n1} & \hat{H}_{s,n2} & \hat{H}_{s,nn} \end{bmatrix}^T \tag{22}$$

$$\hat{P}_C = \begin{bmatrix} \hat{C}_{s,11} & \hat{C}_{s,12} & \cdots & \hat{C}_{s,1n} & \cdots & \hat{C}_{s,n1} & \hat{C}_{s,n2} & \hat{C}_{s,nn} \end{bmatrix}^T \tag{23}$$

$$\hat{P}_G = \begin{bmatrix} \hat{G}_{s,1} & \hat{G}_{s,2} & \cdots & \hat{G}_{s,n} \end{bmatrix}^T \tag{24}$$

Then the estimation error vector can be defined as

$$\tilde{P} = \hat{P} - P \tag{25}$$

In fact, not any combination of H, C and G corresponds to a physical system. Therefore, the first step is to prove that the reduced human model represents a real physical system. It is easy to verify that by proving that $\dot{H}_s - 2C_s$ is a skew-symmetric matrix. In other words, the reduced human model satisfies energy conservation where the detailed derivation is in (Dong, Luo et al. 2010).

We propose a theorem to change the "states of interest" of human body. It is composed of a human attitude control law and a human parameter identification law. In fact, the control process and identification process run at the same time. In the proof of Theorem 2, the global stability is shown by proving that the derivative of the constructed Lyapunov function candidate is less than zero.

Theorem 2

Consider a time-varying system with m-order

$$H_s(t)\ddot{q}_s + C_s(t)\dot{q}_s + G_s(t) = \tau_s(t) \tag{26}$$

without any pre-knowledge about H_s, C_s and G_s. The vector $q_{s,d}$ means the desired states. Define the sliding term s as

$$s = \dot{\tilde{q}}_s + \Lambda\tilde{q}_s = (q_s - q_{s,d})' + \Lambda(q_s - q_{s,d}) \tag{27}$$

where Λ is a positive diagonal matrix. Define the reference velocity $\dot{q}_{s,r}$ and reference acceleration $\ddot{q}_{s,r}$ as

$$\begin{aligned} \dot{q}_{s,r} &= \dot{q}_s - s \\ \ddot{q}_{s,r} &= \ddot{q}_s - \dot{s} \end{aligned} \tag{28}$$

If we choose the human attitude control law

$$\tau_s = \hat{H}_s(t)\ddot{q}_{s,r} + \hat{C}_s(t)\dot{q}_{s,r} + \hat{G}_s(t) - k \cdot \mathrm{sgn}(s) \tag{29}$$

and human parameter identification law

$$\dot{\hat{P}} = -\Gamma^{-1}\left[s_1\ddot{q}_{s,r}{}^T \cdots s_n\ddot{q}_{s,r}{}^T \; s_1\dot{q}_{s,r}{}^T \cdots s_n\dot{q}_{s,r}{}^T \; s_1 \cdots s_n \right] \tag{30}$$

under the assumption of

$$\left\| k \cdot s^T \mathrm{sgn}(s) \right\| > \left\| \tilde{P}^T \Gamma \dot{P} \right\| \tag{31}$$

the human dynamics tracks the desired state trajectory and the parameter estimation H_s, C_s and G_s converge to the actual human parameters asymptotically, where k and Γ are positive diagonal matrixes, $\mathrm{sgn}(\cdot)$ is a signal function.

The proof of Theorem 2 is shown in (Dong, Luo et al. 2010). It is noted that the signals required in the control law and identification law are s, $\dot{q}_{s,r}$, $\ddot{q}_{s,r}$ (Equation (29) and Equation (30)). According to the definitions of s, $\dot{q}_{s,r}$, $\ddot{q}_{s,r}$ (Equation (27) and Equation (28)), the basic signals required are q_s, $\dot{q}_s$, $\ddot{q}_s$. Actually, the "states of interest" q_s, $\dot{q}_s$ represent the basic attitude element of human, i.e. position, angle, linear velocity, angular velocity.

Hence, they are easy for measuring. The measurement can be achieved by binocular vision technology. However, $\ddot{q}_s$ is hard to measure. To avoid the acceleration signal, we use filtering technology. Specifically, let $w(t)$ be the impulse response of a stable, proper filter. For example, for the first-order filter $\varepsilon/(p+\varepsilon)$ where $\varepsilon>0$, $p=d/dt$, the impulse response is $e^{-\varepsilon t}$. Then using partial integration, $\ddot{q}_s$ can be integrated as

$$\begin{aligned}\int_0^t w(t-r)\ddot{q}_s dr &= w(t-r)\dot{q}_s\Big|_0^t - \int_0^t \frac{dw}{dr}\dot{q}_s dr \\ &= w(0)\dot{q}_s - w(t)\dot{q}_s(0) - \int_0^t \left[w(t-r)\dot{q}_s - \dot{w}(t-r)\dot{q}_s\right] dr\end{aligned} \tag{32}$$

which means $\ddot{q}_s = f(\dot{q}_s, w)$, i.e., the acceleration signal can be obtained from velocity signal.

3.5 Simulation

3.5.1 Simulation results

The simulation was implemented by coordination of three software packages, including AUTOLEV, MATLAB and VORTEX. The detailed cooperation relations are explained as follows. AUTOLEV is used to construct the human model (Kane and Levinson 1985). We choose MATLAB to process the main computation of solving ordinary differential equations; Although VORTEX is able to do physical simulation, the programming grammar is a bit complex. Here, we just use its stereoscopic presentation function to make animations.

In the simulation, we choose the head position (denoted as $P_{h,x}$, $P_{h,y}$, $P_{h,z}$), the angle drift off the horizontal line of lower-trunk (denoted as $\theta_{1,x}$, $\theta_{1,y}$, $\theta_{1,z}$), the angle of lower-trunk and upper-leg (denoted as $\theta_{2,x}$, $\theta_{2,y}$, $\theta_{2,z}$) to constitute the "states of interest", i.e.

$$q_s = \left[P_{h,x},\ P_{h,y},\ P_{h,z},\ \theta_{1,x},\ \theta_{1,y},\ \theta_{1,z},\ \theta_{2,x},\ \theta_{2,y},\ \theta_{2,z}\right]^T \tag{33}$$

The initial velocity and acceleration are set as $q_s(0)=\dot{q}_s(0)=0$ and the desired states are set as

$$\begin{aligned}q_{s,d} &= \left[0.2,\ 0.8,\ 0.01,\ 0.01,\ 0.01,\ -0.7854,\ 0.01,\ 0.01,\ 1.5708\right]^T \\ \dot{q}_{s,d} &= \ddot{q}_{s,d} = \left[0,\ 0,\ 0,\ 0,\ 0,\ 0,\ 0,\ 0,\ 0\right]^T\end{aligned} \tag{34}$$

Applying the human attitude control law in Equation (29) and human parameter adaptation law in Equation (30), we obtain

$$\tau_s = \left[F_{h,x},\ F_{h,y},\ F_{h,z},\ \tau_{1,x},\ \tau_{1,y},\ \tau_{1,z},\ \tau_{2,x},\ \tau_{2,y},\ \tau_{2,z}\right]^T \tag{35}$$

Then we choose

$$\begin{aligned}F_1 &= \begin{bmatrix}F_{h,x}\\ F_{h,y}\\ F_{h,z}\end{bmatrix} \\ F_2 &\approx \begin{bmatrix}(\tau_{1,z}l_{1,z}\sin\theta_{1,z} + \tau_{2,z}l_{2,z}\sin\theta_{2,z}) + (\tau_{1,y}l_{1,y}\cos\theta_{1,y} + \tau_{2,y}l_{2,y}\cos\theta_{2,y})\\ (\tau_{1,z}l_{1,z}\cos\theta_{1,z} + \tau_{2,z}l_{2,z}\cos\theta_{2,z}) + (\tau_{1,x}l_{1,x}\sin\theta_{1,x} + \tau_{2,x}l_{2,x}\sin\theta_{2,x})\\ (\tau_{1,x}l_{1,x}\cos\theta_{1,x} + \tau_{2,x}l_{2,x}\cos\theta_{2,x}) + (\tau_{1,y}l_{1,y}\sin\theta_{1,y} + \tau_{2,y}l_{2,y}\sin\theta_{2,y})\end{bmatrix}\end{aligned} \tag{36}$$

where $\left[l_{1,x},\ l_{1,y},\ l_{1,z}\right]^T$ denotes the distance between the head position and the buttock. $\left[l_{2,x},\ l_{2,y},\ l_{2,z}\right]^T$ denotes the distance between the buttock and the application point of F_2. By applying F_1 and F_2, human attitude control is achieved.

The energy, position and angle changes are shown in Fig. 6. It is seen that it takes about 1 second to accomplish the process of attitude change. There is a peak of kinematics energy at the time of about 0.2 second which means at that time, the attitude changes very quickly (Fig. 6 (a)). One reason is that we assume no pre-knowledge of the human body at the beginning of the simulation. The head position changed to the desired (0.2m, 0.8m, 0.01m) at about 1 second (Fig. 6 (b)). Compared with other joints rotating in x or y direction, the joints rotating in z direction change significantly. Thus, the angle changes of these joints affect the head position in x direction greater.

In (Dong, Luo et al. 2010), it is shown that $\dot{H}_s - 2C_s$ is a skew-symmetric matrix which indicates that parts of the states (or their linear combination) can be controlled as a whole. In the simulation, we constructed a new state which is the angle sum of head, chest, mid-trunk, and lower-trunk. The angle drift off the horizontal line of the new state changes to the desired -0.7854 rad (i.e. -45 degrees) at about 1 second as shown in Fig. 6 (c). The angle between lower-trunk and upper-leg changes to the desired 1.5708 rad (i.e. 90 degrees) at about 1 second (Fig. 6 (d)).

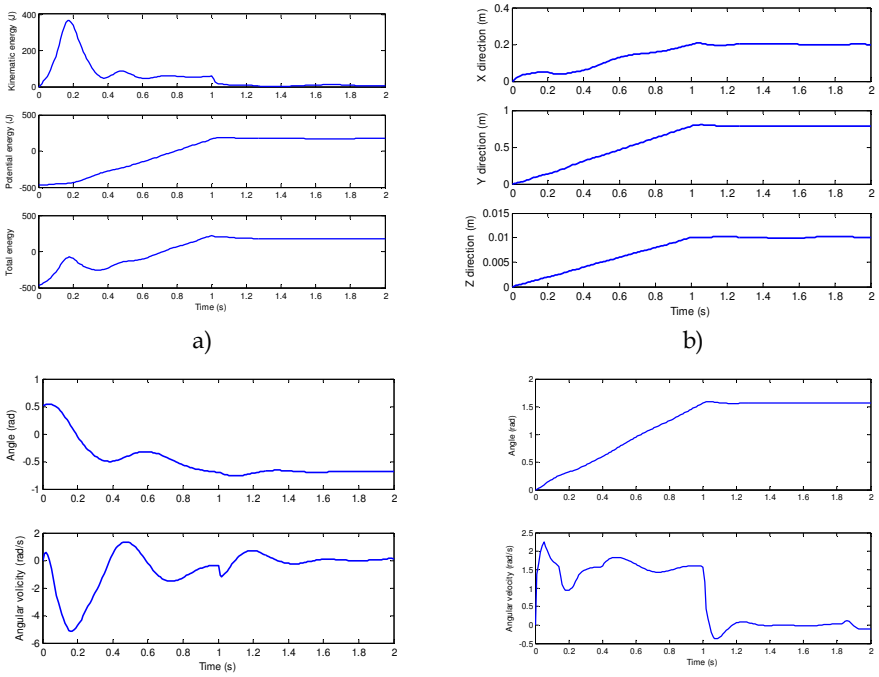

Fig. 6. Energy and angle change.

3.5.2 Animation

We imported the computed motion data into the VORTEX human model to make animation. Here the human model is the visible skeleton which was built in (Dong, Luo et al. 2010). Compared with the human model for simulation (16 links and 35 DOF), the human model for animation is a redundant one (54 links and 61 DOF). Here we just make the corresponding human joints rotate and maintain the redundant human joints fixed. As assumed in the simulation that the force contact type is contingence, we choose two cylindrical objects to represent robot arms.

The position of the head, angle drift off the horizontal line of lower-trunk, angle of lower-trunk and upper-leg are chosen as the "states of interest" (Fig. 7 (a)). The animation of lifting up human by the adaptive force control is shown in Fig. 7 (b) – (f). At the beginning of the simulation, we assume that we do not have any pre-knowledge about the human parameter. Hence, the initial values of $\hat{H}_s$, $\hat{C}_s$ and $\hat{G}_s$ are set to zero matrices (or zero vectors). As the identification of the human parameter goes on, $\hat{H}_s$, $\hat{C}_s$, $\hat{G}_s$ converge to the true values H_s, C_s, G_s.

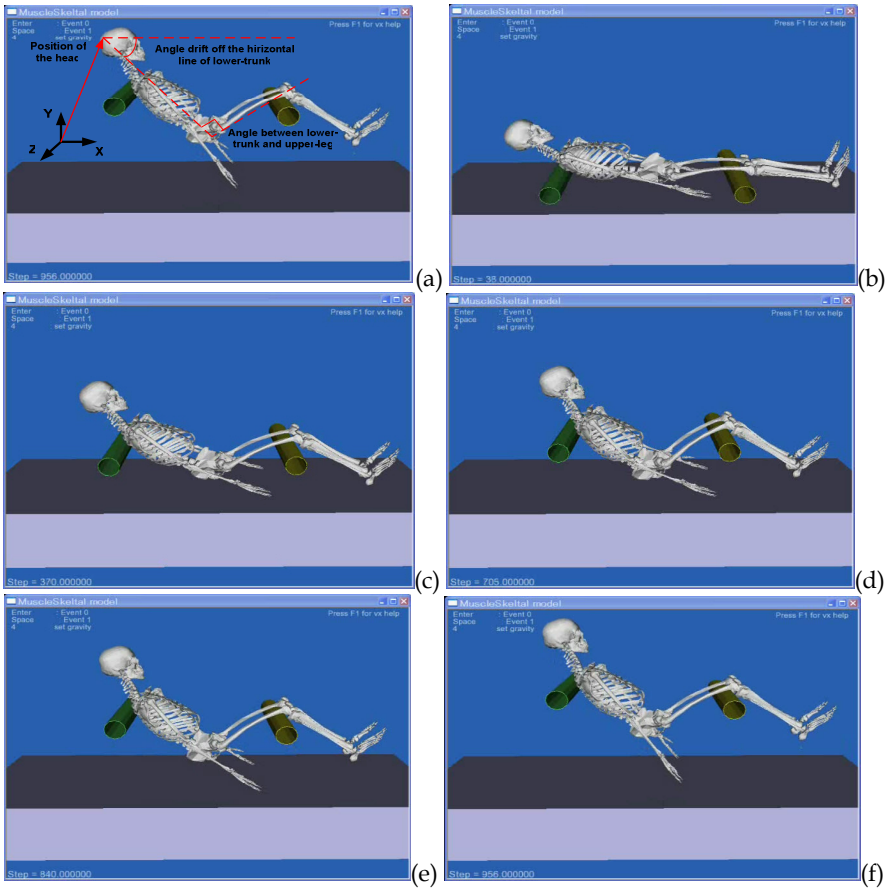

Fig. 7. "States of interest" in lifting human and Snapshots of the lifting human process (Dong, Luo et al. 2010).

3.6 Summary

In this section, an attitude control approach was proposed to lift human without regard to the individual differences, such as height, weight, and so on. We used robust adaptive control to eliminate the effects from the "uninterested joints" and identify the human parameters in real time. In addition, the convergence analysis, including tracking time and static tracking error, was also given. The approach was simulated by lifting a normal human body with two robot arms, which verifies the efficiency and effectiveness of the proposed strategy.

Compared with the previous researches, there are two novelties in the proposed approach. First is that it is not necessary to measure human, like height and weight, in advance because the approach can automatically identify the human parameter online. Second is that the attitude control law ensures the accuracy. Moreover, the robust controller which we proposed also has the ability to tolerate the model uncertainty of human.

Actually, lifting human is a typical problem when interacting with human by force. As human is such a big redundant model, a good solution is to reduce it and design controls. Here, there are two sources of model uncertainties: one is from the unmodeled dynamics which we cannot measure; the other is the generating model uncertainty which comes from model reduction. The effectiveness of the adaptive force control shows that by designing robust controller and online estimator, the two uncertainties mentioned can be solved.

4. Speed control by human's walking intention

4.1 Background

Human walking servo robot is a robot which adaptively adjusts its velocity to human's walking speed. In this section, we consider controlled treadmill as human walking servo robot. In the previous human walking servo robot applications, the subjects had to passively follow the given speed (Mcdermott, Ades et al. 2009; Powell, Stevens et al. 2009). However, in many application cases, the human walking servo robot control strategy motivated by human will is very desirable. However, human will is very complex and hard to be measured. Even if certain models are obtained by brain signal, like brain computer interface (BCI), the models are limited because of great unmodeled uncertainty.

Such a huge unmodeled uncertainty is very difficult to handle. Although the adaptive control with identification can tolerate some degree of unmodeled dynamics, it requires the unmodeled uncertainty is in some degree of limit. Once the model uncertainty is beyond the threshold, the control strategy corrupts. Considering this, we have to find another way which does not rely on model much. One constructive perspective is to consider the human process as a black box with multi-input and multi-output. Based on the experimental approach, we can evaluate the human process by the input stimulation (from u_1 to u_m) and output human response (from x_1 to x_n). The objective is to find a relation f_i to satisfy $x_i = f_i(u_1, \cdots, u_m) \quad 1 \le i \le n$ where f_i can be linear or nonlinear function. By determing f_i $(1 \le i \le n)$, we can evaluate the human process. This section focuses on designing control for human walking servo robot by human's walking intention. As we consider the human process as a multi-input-muilti-output (MIMO) black box, the main topic is to identify the MIMO human process.

4.2 Human walking intention extraction

4.2.1 Characteristic index

The coordinate definition is shown in Fig. 8. Here based on the real product of force plate, we assume that the true origin of the strain gauge force plate is not at the geometric center of the plate surface. There is a pad on the force plate. After a series of calibrations of the true origin, the true origin O' is at $(0,0,h)$.

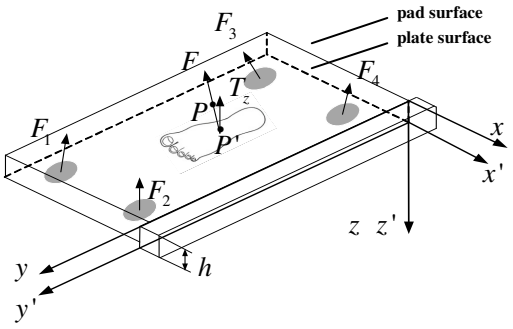

Fig. 8. Coordinate system.

According to the coordinate, the reaction force of ground to feet was simulated where the human model is built by OPENSIM in Section 4.4. It is shown that in one dynamic circle, the force F_z is a bell-shape signal; F_y is a sine-shape signal (Fig. 9 (a)).

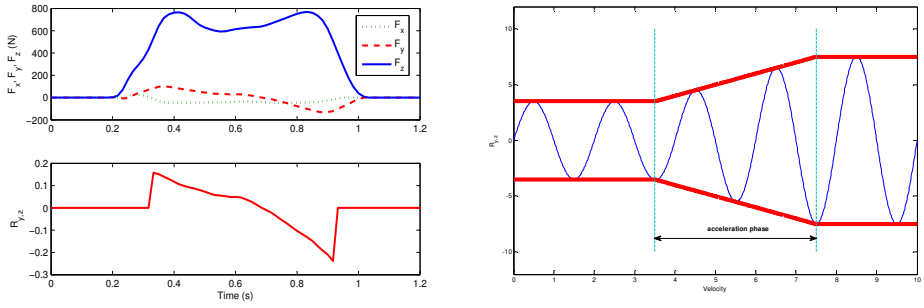

(a) (b)

Fig. 9. Envelope of R_{lyz} in acceleration.

We can explain the reason of such curve shape as follows. When foot gets in touch with the surface of force plate, F_z increases very rapidly. At the same time, foot has to make a break to adjust its speed to the velocity of the force plate by fiction. After break process, foot applies a force with inverse direction to drive the leg to take a step, i.e. make a preparation for higher speed of leg in the next moment. It is noted that, compared with the previous break process, F_y changes its direction at this time. Until now, the foot is on the force plate. Hence, F_z maintains large (for a normal person with 70 kg weight, F_z is about 700 N).

Finally, the subject alternates the other foot to support body and F_z decreases rapidly. Considering the fact that when F_z is large enough, one foot is firmly on the human walking servo robot. We define a ratio index $R_{y,z}$ as

$$R_{y,z} = \begin{cases} \dfrac{F_y}{F_z} & F_z \geq \xi \\ 0 & others \end{cases} \tag{37}$$

where ξ is a threshold. In normal cases, ξ is set as $\max\{F_z\} \times 80\%$. According to the curve shapes of F_y and F_z, the curve shape of $R_{y,z}$ is a composite signal of connection of sine-shape signals and zero signals.

To prove the above simulation result and corresponding analysis, we use Bertec treadmill TM07-B to complete a verification experiment. It is noted that under the treadmill, there are two force plates individually measuring the interaction force and moment. In the experiment, the reaction data are measured when the treadmill velocity varies from 1.0 m/s to 1.6 m/s.

Without loss of generality, the zero signals are ignored in analysis, which leads to that $R_{y,z}$ changes to a connection of various sine-shape signals with different magnitude. It can be inferred that $R_{y,z}$ is a characteristic index for the walking intention: when the subject intends to speed up, $\|R_{y,z}\|_\infty$ becomes large, i.e. both the magnitudes of peak value and valley value become large. After acceleration, $R_{y,z}$ returns to a new equilibrium state (Fig. 9 (b)). In other words, the envelope curve of $R_{y,z}$ determines the intended walking speed. The deceleration case can be explained in a similar way.

4.2.2 Walking intention modeling

To model the characteristic index $\|R_{y,z}\|_\infty$, we use least-squares regression method to identify it. Specifically, first of all define the local peak value $R^+_{y,z}$ and local valley value $R^-_{y,z}$ of $R_{y,z}$ as

$$\begin{aligned} R^+_{y,z} &= \max_{0 \leq t \leq T}\{R_{y,z}\} \\ R^-_{y,z} &= \min_{0 \leq t \leq T}\{R_{y,z}\} \end{aligned} \tag{38}$$

where T is the period of $R_{y,z}$. We can get a sequence of measurements

$$(V_{\text{intend},1}, R^-_{y,z,1}), (V_{\text{intend},2}, R^-_{y,z,2}), \cdots, (V_{\text{intend},n}, R^-_{y,z,n}) \tag{39}$$

Assuming that $R^-_{y,z}$ is predicted as a function of the intended walking speed V_{intend}, then one can model this situation by

$$R^-_{y,z} = f_w(V_{\text{intend}}, \lambda_w) + \varepsilon_w \tag{40}$$

where λ_w is a parameter vector. The random variable ε_w is independent of V_{intend} and on average it is equal to zero, i.e. $E(\varepsilon_w) = 0$. We want to find f_w that fits the measurement data best and we define the loss function to measure the quality of the fit as

$$L = \left\| R_{y,z}^{-} - f_w(V_{\text{intend}}, \lambda_w) - \varepsilon_w \right\|_2 \tag{41}$$

We minimize it over all choices of parameter vector λ_w. To find the approximation function, we write

$$\frac{\partial L\left(R_{y,z}^{-}, f_w(V_{\text{intend}}, \lambda_w), \varepsilon_w\right)}{\partial \lambda_w} = 0 \tag{42}$$

In this section, we choose the other three model candidates: quadratic, cubic, 4th degree polynomial. In the experiment, we obtain $R_{y,z}$ ten times when the treadmill velocity varies from 0.1 m/s to 1.0 m/s. The observation samples are shown in Table 1.

Velocity (m/s)	$R_{y,z}^{+}$	$R_{y,z}^{-}$	Velocity (m/s)	$R_{y,z}^{+}$	$R_{y,z}^{-}$
0.1	0.0080	-0.0213	0.6	0.0872	-0.1172
0.2	0.0310	-0.0353	0.7	0.1078	-0.0834
0.3	0.0716	-0.0542	0.8	0.1126	-0.1224
0.4	0.0622	-0.0695	0.9	0.1153	-0.1187
0.5	0.0957	-0.0884	1.0	0.1841	-0.1421

Table 1. Observation samples.

For the purpose of evaluating the candidate models, we define residual norm as the sum of square of deviations

$$S_r = \sum_{i=1}^{n} \left\| R_{y,z,i}^{-} - \hat{R}_{y,z}^{-} \right\|_2 = \sum_{i=1}^{n} \left\| R_{y,z,i}^{-} - f_w\left(V_{\text{intend}}, \hat{\lambda}_w\right) \right\|_2 \tag{43}$$

where $\hat{R}_{y,z}^{-}$ is the estimation of $R_{y,z}^{-}$ based on the particular model. Take linear model for example, $\hat{R}_{y,z}^{-} = \hat{\lambda}_{w,0} + \hat{\lambda}_{w,1} V_{\text{intend}}$. The regression results are shown in Table 2.

Regression Model	Results	Norm of Residuals
linear	$R_{y,z}^{-} = -0.13 V_{\text{intend}} - 0.011$	0.039887
quadratic	$R_{y,z}^{-} = 0.067 {V_{\text{intend}}}^2 - 0.2 V_{\text{intend}} - 0.00072$	0.034701
cubic	$R_{y,z}^{-} = -0.08 {V_{\text{intend}}}^3 + 0.19 {V_{\text{intend}}}^2 - 0.25 V_{\text{intend}} + 0.0022$	0.034094
4th degree polynomial	$R_{y,z}^{-} = -0.6 {V_{\text{intend}}}^4 + 1.1 {V_{\text{intend}}}^3 - 0.56 {V_{\text{intend}}}^2 - 0.097 V_{\text{intend}} - 0.0021$	0.031844

Table 2. Regression results.

Because the residual norms of the four types do not have big difference, any model of the four is able to describe the human's intended walking speed. Therefore, for simplicity we choose the linear model as follows.

$$R_{y,z}^{-} = -0.13 \cdot V_{\text{intend}} - 0.011 \tag{44}$$

To summarize, the human walking intention is extracted in four steps as follows. The first step is to collect a sequence of measurements $(V_{\text{intend},1}, R_{y,z,1}^{-}), \cdots, (V_{\text{intend},n}, R_{y,z,n}^{-})$. The second step is to select a model type for intended walking speed based on Equation (40). Take linear model for example, $R_{y,z}^{-} = \lambda_{w,0} + \lambda_{w,1} V_{\text{intend}}$. The third step is to define the loss function (Equation (41)) and compute the estimation of unknown coefficients. In the case of linear model, $\hat{\lambda}_{w,0}$ and $\hat{\lambda}_{w,1}$ are derived in (Dong, Luo et al. 2010). The fourth step is to compute the residual norms of the candidate models (Equation (46)). Considering model complexity and accuracy, choose a proper model.

4.3 Adaptive speed control

Nowadays human walking servo robot's application has become more and more popular in many fields like athletic exercise, rehabilitation training. In the following part, a speed control by human's walking intention is proposed by which the subject control the speed of human walking servo robot at his (or her) will.

4.3.1 System construction

The human walking servo robot used in the application is Bertec treadmill TM07-B. When the user walks on the treadmill, the dual force plates (placed under the human walking servo robot) measure the force and moment signals in x, y, z directions as F_x, F_y, F_z, M_x, M_y, M_z and output them as analog signals. After amplifying them and doing analog-to-digital (A/D) conversion, the digital signals are transferred to PC. Based on the force signals, human's walking intention is identified by the least-squares method illustrated in Section 4.2.2. Then the human's intended walking speed is used to drive the motors corresponding with left belt speed control and right belt speed control, respectively (Fig. 10). Here from the viewpoint of control, the control plant is Bertec treadmill TM07-B which is controlled by the inner speed controller in the inner loop feedback (Dong, Oshiumi et al. 2010).

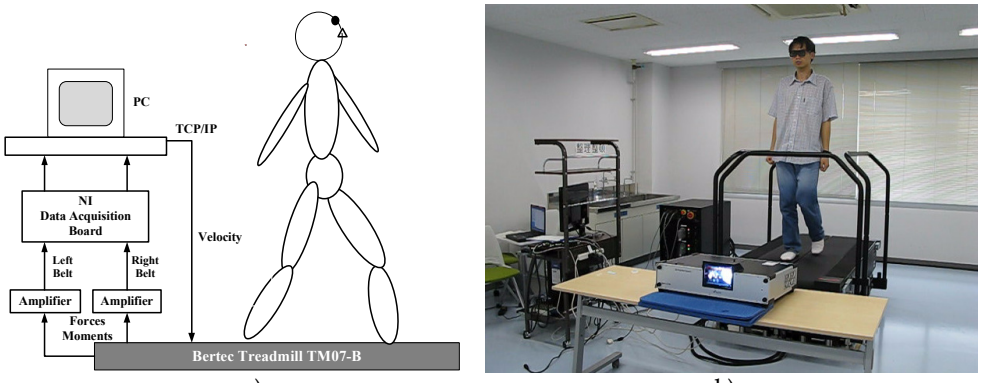

a) b)

Fig. 10. System construction of human walking servo robot.

When the subject walks on the treadmill, there is some kind of perturbation adding to the control signal. It is noted that our control objective is to control the treadmill by human's intended walking speed. Hence, we have to establish an outer loop feedback between the subject's intended speed V_{intend} and the treadmill's inner speed controller.

4.3.2 Experiment results

To calculate the transfer function $G(s)$, we use the characteristic index of intended walking speed in Equation (44). Hence, the intended walking speed is calculated as follows.

$$V_{\text{intend}}(k)=\begin{cases}V_{\text{intend}}(k-1) & R_{y,z}^{-}(k)=0\\ -\left(R_{y,z}^{-}(k)+0.011\right)/0.13 & others\end{cases} \tag{45}$$

There are many reasons, like sensor noise, causing computed intended walking speed not smooth. Here, we choose a delay-line filter to solve the problem. Finally, the intended walking speed driving the treadmill's inner controller is

$$V_{\text{treadmill}}(k)=\frac{1}{4}\sum_{i=1}^{4}V_{\text{intend}}(k-i) \tag{46}$$

Good performance can be obtained by using the above filter for many times. Fig. 11 shows a dynamic walking process with acceleration motion, deceleration motion and uniform motion (constant speed motion) in the time interval $[28,34]$, $[55,65]$, $[15,24]$, respectively.

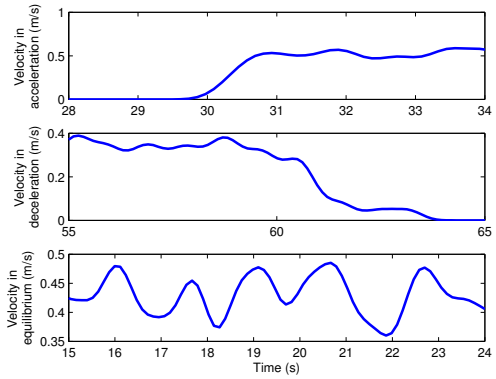

Fig. 11. Speed control result.

4.4 Summary

This section proposed a method for extracting human's walking intention and based on it, a speed control was proposed for adaptively driving human walking servo robot by human's will. The ground reaction force is considered as the indicator of the human's intended walking speed. By analyzing the walking simulation, we found a characteristic index which has significant relevance with the intended walking speed. After processing least-squares regression, four kinds of candidate models were obtained. For simplicity, we chose the

linear model. The extracted human intention was used to control the human walking servo robot. The control performance shows the effectiveness of the proposed method for extracting human walking intention.

Compared with previous researches, there are two novelties to be illustrated. First is that the proposed method for human walking intention extraction simply uses the ground reaction forces to do estimation. The method is so easy-to-use that it even can be used on single-chip. The second is that in the previous human walking servo robot control, the subject had to follow the speed of human walking servo robot passively. While the proposed speed control can adaptively adjust the velocity of human walking servo robot to the subject's, which shows great potential both in research and real-world applications.

Actually, when HIR interacts with human by human's intention, it is extremely hard to model or identify the unmodeled uncertainty because we know so little about human's intention. In this case, it is a good way to analyze it just from the relation between inputs and outputs. The proposed speed control based on human's walking intention shows that by identifying the relation mentioned, we can deal with the unmodeled uncertainty from human's intention.

5. Conclusion

In this chapter, we designed kinds of control strategies of HIR and solved three typical problems for HIR. A sparse extended information filter SLAM approach was proposed for HIR's navigation in a large unknown environment, which ensures HIR can fulfil its task in human surrounding environments. An adaptive force control was designed for HIR To lift human solving the physical interaction under an uncertainty of human dynamics of dealing with the complex human dynamics during interaction. A speed control by human's intended walking speed was designed, which gives a solution to extracting human's intention. Compared with other HIR approach, this chapter takes fully into account of uncertainties HIR encounters, including environment uncertainty, sensor uncertainty, actuator uncertainty, model uncertainty and unmodeled uncertainty. The contribution of this chapter is not only to give specific HIR controls for specific cases, but also to provide a good solving framework for HIR problem.

6. References

Dong, H., Z. Luo, et al. (2009). Sparsing of information matrix for practical application of a robot's SLAM. IEEE/RSJ International Conference on Robotics and Automaion.

Dong, H., Z. Luo, et al. (2009). Sparsing of information matrix for practical application of a robot's SLAM. IEEE/RSJ International Conference on Robotics and Automation.

Dong, H., Z. Luo, et al. (2010). "Adaptive attitude control for redundant time-varying complex model of human body in the nursing activity." Journal of Robotics and Mechatronics 22(4): 418-429.

Dong, H., Z. Luo, et al. (2010). "Adaptive attitude control for redundant time-varying complex model of human body in the nursing activity." Japanese Journal of Biomechanics in Sports and Exercise 14(1): 52-60.

Dong, H., Z. Luo, et al. (2010). Adaptive treadmill control by human will. 13th International Conference on Climbing and Walking Robots and the Support Technologies for Mobile Machines.

1 Dong, H., Z. Luo, et al. (2010). Reduced model adaptive control for carrying human beings
2 with uncertain body dynamics in nursing care. IEEE/ASME International
3 Conference on Advanced Intelligent Mechatronics.
4 Dong, H., T. Oshiumi, et al. (2010). Development of a 3D interactive virtual market system
5 with adaptive treadmill control. IEEE/RSJ International Conference on Intelligent
6 Robots and Systems.
7 Dong, H., J. Tang, et al. (2010). "A novel information matrix sparsification approach for
8 practical implementation of SLAM." Advanced Robotics 24(5-6): 819-838.
9 Eustice, R., H. Singh, et al. (2006). "Exactly sparse delayed-state filters for view based
10 SLAM." IEEE Transactions on Robotics 22: 1100-1114.
11 Eustice, R., M. Walter, et al. (2005). Sparse extended information filters: insights into
12 sparsification. IEEE International Conference on Intelligent Robots and Systems.
13 Eustice, R. M., H. Singh, et al. (2005). Exactly sparse delayed-state filters. IEEE International
14 Conference on Robotics and Automation.
15 Kane, T. R. and D. A. Levinson (1985). Dynamics: Theory and Applications, McGraw-Hill.
16 Liu, Y. F. and S. Thrun (2003). Results for outdoor-SLAM using sparse extended information
17 filters. IEEE International Conference on Robotics and Automation.
18 Mcdermott, M. M., P. Ades, et al. (2009). "Treadmill exercise and resistance training in
19 patients with peripheral arterial disease with and without intermittent claudication:
20 a randomized control trail." Journal of American Medical Association 301: 165-174.
21 Mukai, T., M. Onishi, et al. (2008). "Development of the tactile sensor system of a human-
22 interactive robot "RI-MAN"." IEEE Transactions on Robotics 24: 505-512.
23 Onish, M., Z. W. Luo, et al. (2007). Generation of human care behaviors by human-
24 interactive robot RI-MAN. IEEE International Conference on Robotics and
25 Automation.
26 Powell, W., B. Stevens, et al. (2009). "Treadmill interface for virtual reality vs. overground
27 walking: a comparison of gait in individuals with and without pain."
28 Cyberpsychology and Behavior 12.
29 Smith, R., M. Self, et al. (1990). Estimating Uncertain Spatial Relationships in Robotics,
30 Springer-Verlag.
31 Thrun, S., W. Burgard, et al. (2005). Probabilistic Robotics, The MIT Press.
32 Thrun, S., D. Koller, et al. (2002). Simultaneous Mapping and Localization with Sparse
33 Extended Information Filters: Theory and Initial Results, Carnegie Mellon
34 University.
35 Thrun, S., Y. Liu, et al. (2004). "Simultaneous localization and mapping with sparse extended
36 information filters." International Journal of Robotics Research 23: 693-716.